JOURNAL OF VIROLOGY, July 2009, p. 7221–7234 Vol. 83, No. 14
0022-538X/09/$08.00+0 doi:10.1128/JVI.00440-09

Identification of In Vivo-Interacting Domains of the Murine Coronavirus Nucleocapsid Protein▽

Kelley R. Hurst, Cheri A. Koetzner, and Paul S. Masters*

Wadsworth Center, New York State Department of Health, Albany, New York 12201

Received 2 March 2009/Accepted 27 April 2009

The coronavirus nucleocapsid protein (N), together with the large, positive-strand RNA viral genome, forms a helically symmetric nucleocapsid. This ribonucleoprotein structure becomes packaged into virions through association with the carboxy-terminal endodomain of the membrane protein (M), which is the principal constituent of the virion envelope. Previous work with the prototype coronavirus mouse hepatitis virus (MHV) has shown that a major determinant of the N-M interaction maps to the carboxy-terminal domain 3 of the N protein. To explore other domain interactions of the MHV N protein, we expressed a series of segments of the MHV N protein as fusions with green fluorescent protein (GFP) during the course of viral infection. We found that two of these GFP-N-domain fusion proteins were selectively packaged into virions as the result of tight binding to the N protein in the viral nucleocapsid, in a manner that did not involve association with either M protein or RNA. The nature of each type of binding was further explored through genetic analysis. Our results defined two strongly interacting regions of the N protein. One is the same domain 3 that is critical for M protein recognition during assembly. The other is domain N1b, which corresponds to the N-terminal domain that has been structurally characterized in detail for two other coronaviruses, infectious bronchitis virus and the severe acute respiratory syndrome coronavirus.

The assembly of coronaviruses is driven principally by homotypic and heterotypic interactions between the two most abundant virion proteins, the membrane protein (M) and the nucleocapsid protein (N) (14, 32). The M protein is a triple-spanning transmembrane protein residing in the virion envelope, which is derived from the cellular budding site, the endoplasmic reticulum-Golgi intermediate compartment. More than half of the M molecule, its carboxy-terminal endodomain, is situated in the interior of the virion, where it contacts the nucleocapsid (46, 50). Also found in the virion envelope is the spike protein (S), which, although crucial for viral infectivity, is not an essential participant in assembly. The other canonical component of the coronavirus envelope is the small envelope protein (E), the function of which is enigmatic. Some evidence suggests that the E protein does not make sequence-specific contacts with other viral proteins (27) but instead functions by modifying the budding compartment, perhaps as an ion channel (56, 57). Alternatively, or additionally, E could act in a chaperone-like fashion to facilitate homotypic interactions between M protein monomers or oligomers (4).

The N protein is the only protein constituent of the helically symmetric nucleocapsid, which is located in the interior of the virion. Coronavirus N proteins are largely basic phosphoproteins that share a moderate degree of homology across all three of the phylogenetic groups within the family (29). Some time ago, we proposed a model that pictured the N protein as comprising three domains separated by two spacers (A and B) (40). This arrangement was originally inferred from a sequence comparison of the N genes of multiple strains of the prototypical group 2 coronavirus, mouse hepatitis virus (MHV), and its validity seemed to be reinforced by numerous sequences that later became available. Part of this model, the delineation of spacer B and the acidic, carboxy-terminal domain 3, has been well supported by subsequent work (22, 25, 41, 42). However, a wealth of recent, detailed structural studies of bacterially expressed domains of the N proteins of the severe acute respiratory syndrome coronavirus (SARS-CoV) and of infectious bronchitis virus (IBV) has much more precisely mapped boundaries within the remainder of the N molecule (8, 16, 21, 23, 47, 51, 60). The latter studies have shown that the N protein contains two independently folding domains, designated the N-terminal domain (NTD) and the C-terminal domain (CTD). It should be pointed out that this nomenclature can be misleading: the NTD does not contain the amino terminus of the protein, and the CTD does not contain the carboxy terminus of the protein. Specifically, the CTD does not include spacer B and domain 3. The NTD and the CTD are separated by an intervening serine- and arginine-rich region; this region was previously noted to resemble the SR domains of splicing factors (42), and it has recently been shown to be intrinsically disordered (6, 7).

In the assembled virion, the three known partners of the N protein are the M protein, the genomic RNA, and other copies of the N protein itself. We have sought to develop genetic and molecular biological methods that will begin to elucidate the varied ways in which the N molecule interacts during MHV infection. We previously found that the fusion of N protein domain 3 to a heterologous marker, green fluorescent protein (GFP), results in incorporation of GFP into virions (22). In the present study, we similarly fused each of the individual domains of N to GFP, and we thereby uncovered two strong modes of N protein-N protein interaction that likely contribute to virion architecture.

* Corresponding author. Mailing address: David Axelrod Institute, Wadsworth Center, NYSDOH, New Scotland Avenue, P.O. Box 22002, Albany, NY 12201-2002. Phone: (518) 474-1283. Fax: (518) 473-1326. E-mail: masters@wadsworth.org.

▽ Published ahead of print on 6 May 2009.

MATERIALS AND METHODS

Cells and viruses. Wild-type MHV-A59 and MHV mutants were propagated in mouse 17 clone 1 (17Cl1) cells; plaque assays and plaque purifications of mutant recombinants and revertants were carried out in mouse L2 cells. The interspecies chimeric virus designated fMHV.v2 (19) was grown in feline FCWF cells.

Targeted RNA recombination. All MHV mutants were isolated through targeted RNA recombination, using the host-range-based selection described in detail previously (19, 22, 26–28). In brief, monolayers of FCWF cells were infected with fMHV.v2 and were then transfected with synthetic donor RNAs that had been generated by transcription with T7 RNA polymerase (mMessage mMachine; Ambion), using PacI-truncated plasmid templates. Resulting progeny virus was harvested at 24 to 48 h postinfection, and recombinant candidates were selected and purified by two rounds of plaque titration on mouse L2 cell monolayers. For analysis of each recombinant candidate, total RNA was extracted from infected 17Cl1 cell monolayers (Ultraspec reagent; Biotecx), and reverse transcription of RNA was carried out with a random hexanucleotide primer and avian myeloblastosis virus reverse transcriptase (Life Sciences). To ascertain the presence of incorporated mutations or genes, PCR amplifications of cDNAs were performed with AmpliTaq polymerase (Roche), using primer pairs flanking the relevant regions of the genome. Reverse transcription-PCR products were analyzed directly by agarose gel electrophoresis and were purified with QIAquick spin columns (Qiagen) prior to DNA sequencing.

All transcription vectors for synthesis of donor RNAs were ultimately derived from pMH54 (26), which encodes 5′ elements of the MHV genome linked to the 3′-most 8.6 kb of the MHV genome, a region that encompasses all of the structural protein genes. Insertions, mutations, and rearrangements were generated, often via subclones, by means of either direct PCR or PCR-based mutagenesis methods. To produce vectors encoding GFP-N-domain fusion proteins that replace most of accessory gene 4, we modified the previously described pMH54GFP-d3 (22), which in turn had been constructed from pMH54GFP (12). The distance between the transcription-regulating sequence and the GFP start codon in pMH54GFP-d3 was reduced from 82 to 17 bases, so as to shorten the 5′ untranslated region of the corresponding subgenomic mRNA and to facilitate subsequent DNA manipulations; this modification also yielded a small increase in GFP expression. The resulting plasmid, pG1-Nd3, retained two features from its parent plasmid: (i) a two-amino-acid spacer (SG), which created a unique BspEI site between the GFP open reading frame (ORF) and the start of the N gene segment, and (ii) a unique NotI site immediately downstream of the fusion protein ORF. PCR-generated fragments were then used to replace the BspEI-NotI fragment of pG1-Nd3, to produce a set of vectors encoding the other GFP-N-domain fusions, pG1-N1a, pG1-N1b, pG1-N2a, pG1-N2b, and pG1-NBd3. Mutants (mut1 to mut3) of pG1-N1b were created by splicing overlap extension-PCR (20), exchanging the BspEI-NotI fragment of pG1-Nd3. The same N1b mutations were created in the native N gene by replacing the fragment between the M gene BssHII and N gene NheI sites in pSG6, a vector which is identical to pMH54, except that pSG6 contains a coding-silent BspEI site that spans codons 444 to 446 of the N gene (19). Mutations NBd3-PR and NBd3-CCA in spacer B of the N protein were constructed from PCR assembly of multiple oligonucleotides in a pSG6-derived subclone, with insertion of the synthetic fragment between the BstXI site at the start of spacer B and the BspEI site at the end of domain 3. The mutations were then transferred either to pSG6, via exchange of the N gene NheI-BspEI fragment, or else to pG1-Nd3, via a PCR-generated fragment that was used to replace the BspEI-NotI fragment.

Transcription vector pA112, used for generation of the N duplication-tagged recombinant, was constructed in multiple steps. A subclone, pA104, was built that contained the 3′ end of the M gene and the entire N gene, with the following modifications with respect to the wild type: (i) the BssHII site of the M gene was replaced with an SbfI site; (ii) the hemagglutinin (HA) epitope tag, YPYDVP DYA, replaced amino acids 386 to 394 of spacer B of the N gene; (iii) a His_6 epitope tag was appended to the carboxy terminus of the N ORF; and (iv) an XbaI site was created immediately downstream of the N ORF. The SbfI-XbaI fragment of pA104 was then exchanged for the SbfI-SnaBI fragment of pMH54, thereby replacing most of accessory gene 4 with the duplicated N ORF in the resulting clone, pA112. Removal of the downstream copy of the N ORF of pA112, by splicing overlap extension-PCR, generated pA119, the transcription vector for the N transposition-tagged recombinant. Next, replacement of the epitope tags of pA119 with a PCR-generated wild-type N fragment generated pA122, the transcription vector for the N transposition-untagged recombinant. The sequences of the newly created junction downstream of the S ORF (common to pA112, pA119, and pA122), the junction downstream of the duplicated N ORF (common to pA112, pA119, and pA122), and the junction between the M ORF and the 3′ untranslated region (common to pA119 and pA122) have been reported previously (see Fig. 3 in reference 15). Eighteen separate in-frame deletions within the duplicated N ORF were created in the subclone pA104, through religation of blunted ends that had been produced subsequent to digestion with various pairs of the following restriction enzymes: NheI, SpeI, PspOMI, XhoI, NgoMIV, BstXI, ApaI, Bsu36I, BtgI, BlpI, NaeI, BsiWI, and BsrGI. The SbfI-XbaI fragment of each pA104 deletion mutant was then used to replace the SbfI-XbaI fragment of pA112.

All DNA cloning and manipulations were carried out by standard techniques (48). Oligonucleotides for PCR, fragment construction, and DNA sequencing were obtained from Integrated DNA Technologies. The compositions of all plasmid constructs were initially verified by restriction analysis. Then, all PCR-generated segments, cloned cDNA precursors, and reconstructed or newly created junctions of each plasmid were confirmed by DNA sequencing.

Virus purification and fractionation. Purification of MHV with glycerol-tartrate gradients was performed as described in detail previously (58). In brief, polyethylene glycol-precipitated virus was banded by two cycles of equilibrium centrifugation on preformed gradients of 0 to 50% potassium tartrate osmotically counterbalanced with 30 to 0% glycerol, in a buffer of 50 mM Tris-maleate (pH 6.5) and 1 mM EDTA (TME buffer). Purification of MHV by sucrose flotation was carried out as detailed previously (26, 27, 52). In brief, polyethylene glycol-precipitated virus was suspended in a final concentration of 50% sucrose in 20 mM Tris-HCl (pH 7.2) and 20 mM $MgCl_2$ and was floated via equilibrium centrifugation through layers of 48% and 40% sucrose to an interface with 30% sucrose.

Virions that had been purified by the glycerol-tartrate method were fractionated essentially as described previously (50). The relative concentrations of each virus were normalized by protein determination (bicinchoninic acid assay; Pierce), which was confirmed by Western blotting with anti-N monoclonal antibody. Virions (350 ng) were incubated at 4°C for 45 min with 0.25% Nonidet P-40 (NP-40) in TME (50 mM Tris maleate, pH 6.5, 1 mM EDTA) containing either 100 mM or 250 mM NaCl in a total volume of 2 ml. Samples were then layered on top of 2 ml of the same buffer containing 30% glycerol and centrifuged at 208,000 × *g* in a Beckman SW60 rotor at 4°C for 2 h. The pellet was dissolved in sodium dodecyl sulfate-polyacrylamide gel electrophoresis (SDS-PAGE) sample buffer and divided between two gels for Western blot analyses. As an indicator of the amounts of the M and N proteins in unfractionated virions, a control sample of one virus, GFP-N1a, was treated identically throughout the incubation and centrifugation steps, except that NP-40 was omitted from all solutions.

Western blotting and immunoprecipitation. For cell lysate preparation, confluent monolayers (20 cm^2) of 17Cl1 cells were mock infected or were infected with MHV (wild type or constructed mutants) at a multiplicity of 0.25 PFU per cell; cells were then incubated at 37°C for 18 to 28 h. Monolayers were washed twice with phosphate-buffered saline and then lysed by addition of 500 μl of 50 mM Tris-HCl, pH 8.0, 150 mM NaCl, 1.0% NP-40, 0.7 μg/ml pepstatin, 1.0 μg/ml leupeptin, 1.0 μg/ml aprotinin, and 0.5 mg/ml Pefabloc SC (Roche). Lysates were held for 15 min on ice and were then clarified by centrifugation. Samples of either infected cell lysates, purified virions, or fractionated virions were separated by SDS-PAGE through 7.5, 10, or 15% polyacrylamide gels with prestained protein standards (Invitrogen) in flanking lanes and were transferred to polyvinylidene difluoride membranes. Blots were then probed with the indicated antibodies, and bound primary antibodies were visualized using a chemiluminescent detection system (ECL; Amersham).

For immunoprecipitation sample preparation, confluent 17Cl1 cell monolayers (20 cm^2) were infected with MHV at a multiplicity of 1 to 2 PFU per cell for 10 h at 37°C. Following 1 h of starvation in methionine-free medium, cells were labeled for 1 h in 1 ml of methionine-free medium containing 100 μCi of [^{35}S]methionine (Amersham) per ml. Lysates were prepared as described above, precleared with preimmune serum, and then immunoprecipitated with the indicated antibody. For both the preclearing and immunoprecipitation steps, antibodies were adsorbed and collected with *Staphylococcus aureus* protein A-Sepharose 4 beads (Pharmacia). Samples were analyzed by SDS-PAGE, followed by autoradiography.

Antibodies used for Western blot assays or immunoprecipitations were anti-N monoclonal antibody J.3.3 and anti-M monoclonal antibody J.1.3 (both provided by John Fleming, University of Wisconsin, Madison), antihemagglutinin (anti-HA) epitope tag monoclonal antibody (12CA5; Roche), polyclonal rabbit antiserum raised against a bacterially expressed maltose binding protein-MHV N protein fusion, and anti-GFP monoclonal antibody (Clontech).

Northwestern blotting. RNA binding by proteins in cell lysates or purified virions was analyzed as described previously (3, 44, 49), with some modifications. RNA probes were prepared by runoff T7 RNA polymerase transcription of

AvrII-linearized pB36 or MluI-linearized pB1, using a Maxiscript kit (Ambion). Plasmid pB36 encodes a defective-interfering RNA (33); the probe obtained from pB36 consisted of the 5′ 469 nucleotides of the MHV genome, followed by a 46-nucleotide polylinker sequence. Plasmid pB1 contains the smaller HindIII-MluI fragment of nsp15 cloned into pGEM7Zf (Promega); the probe obtained from pB1 consisted of nucleotides 20101 to 20501 of the MHV genome, preceded by a 71-nucleotide polylinker sequence. Probes were labeled with [α-^{32}P]UTP (Amersham) to specific activities of approximately 2×10^6 μCi/μmol and were purified by treatment with RNase-free DNase, followed by phenol-chloroform extraction and ethanol precipitation.

Protein samples were separated by SDS-PAGE through 7.5% or 10% polyacrylamide gels and transferred to polyvinylidene difluoride membranes. Blots were blocked by incubation in standard binding buffer (SBB; 10 mM Tris-HCl, pH 7.0, 50 mM NaCl, 1 mM EDTA, 1 mM dithiothreitol, 0.02% Ficoll 400, 0.02% polyvinylpyrrolidone, 0.02% bovine serum albumin) containing 1 mM UTP and 40 μg/ml unlabeled competitor RNA (total cytoplasmic RNA purified from 17Cl1 cells) at ambient temperature with constant agitation for 90 min. Blots were probed with 2×10^6 cpm/ml of labeled RNA in SBB containing 1 mM UTP and unlabeled competitor RNA at ambient temperature with constant agitation for 90 min. Blots were then washed four times with SBB (15 min for each wash) and dried, and bound RNA was visualized by autoradiography.

RESULTS

Design and expression of GFP-N-domain fusion proteins. To begin to dissect MHV N protein domain interactions in the context of a viral infection, we constructed a set of GFP fusion proteins that collectively spanned the N molecule. Our choice of boundaries for putative domains was based on our previous work with the MHV N protein (22, 25, 40, 42), as well as on recent structural studies of other coronavirus N proteins (6, 8, 16, 21, 23, 47, 60). Accordingly, the N protein was divided into five segments: N1a, N1b, N2a, N2b, and NBd3 (Fig. 1A). The constructs GFP-N1b and GFP-N2b contained aligned segments of the MHV N protein corresponding, respectively, to the NTDs and CTDs that were defined for the N proteins of IBV (16, 23) and SARS-CoV (8, 21, 47, 60). The fusion protein construct GFP-NBd3, which we reported previously (22), contained the carboxy-terminal domain 3 of the N molecule preceded by the hinge or spacer region that has been designated spacer B (25, 40). A shorter version of this construct that lacks spacer B and is designated GFP-d3 was also generated for use in some experiments. The two remaining constructs, GFP-N1a and GFP-N2a, contained the amino terminus of N and the region linking the NTD and the CTD, respectively.

MHV recombinants expressing each of the GFP fusion proteins were generated through targeted RNA recombination, a method by which site-specific changes are engineered into coronavirus genomes via recombination between a synthetic donor RNA and a recipient virus that is subjected to counterselection (25, 34). To accomplish this, we inserted the gene for each GFP fusion protein into a derivative of the transcription vector pMH54 (26) in place of MHV accessory gene 4, which is nonessential (13, 39). Recombinants were then isolated by host-range-based selection, using the interspecies chimeric coronavirus fMHV (19, 26) (Fig. 1B). Western blot analysis of lysates from cells infected with these recombinants and a GFP control virus (12, 22) showed abundant and roughly comparable expression of the expected GFP-N-domain fusion proteins, which were detected by anti-GFP antibody (Fig. 1C). GFP and fusion proteins had somewhat lower SDS-PAGE mobilities than would be expected for their respective molecular masses (27 kDa for GFP, 32 kDa for GFP-N1a, 47 kDa for GFP-N1b, 33 kDa for GFP-N2a, 40 kDa for GFP-N2b, 35 kDa for GFP-NBd3, and 32 kDa for GFP-Nd3), as we and others have noted before (12, 17, 22).

Incorporation of GFP-N-domain fusion proteins into MHV virions. We previously found that attachment of N protein domain 3 to GFP (with or without an intervening spacer B) was sufficient to target GFP for assembly into virions (22). It was therefore of interest to test whether any of the other GFP-N-domain fusion proteins were specifically associated with assembled virions. As a preliminary step, we compared two methods of virion purification for this purpose: one in which virions were banded by two consecutive rounds of equilibrium sedimentation on glycerol-tartrate gradients (58) and one in which virions were banded by flotation through successive layers of sucrose of decreasing density (27, 52). As shown in Fig. 2A for the GFP and GFP-N1a recombinants, the glycerol-tartrate gradient method in our hands yielded virus preparations of much higher purity. Similar results were obtained for all six recombinant viruses (data not shown).

Analysis of glycerol-tartrate gradient-purified virions by Western blotting revealed that, of the five GFP fusion constructs spanning the N molecule, there was substantial incorporation of GFP-N1b and, as observed previously, of GFP-NBd3 (22) (Fig. 2B). We also consistently observed a minor amount of incorporation of GFP-N2b into virions. In contrast, there was no virion incorporation of GFP alone, nor of either the GFP-N1a or the GFP-N2a fusion protein. This result suggested that the packaging of GFP-N1b, GFP-NBd3, and GFP-N2b into MHV was specifically due to the particular N domain that was attached to each of them.

Fractionation of virions containing GFP-N-domain fusion proteins. To further probe the nature of the association of GFP-N-domain fusion proteins with virions, we used the MHV fractionation procedure developed by Sturman and coworkers (50). Purified virions were incubated at 4°C with 0.25% NP-40 in buffer containing 100 mM NaCl, a condition previously shown to solubilize the virion membrane envelope, including the S glycoprotein, and to abolish the interaction of the M protein with the nucleocapsid. Nucleocapsids were then collected by centrifugation through a layer of 30% glycerol in the same buffer, which also contained 0.25% NP-40 and 100 mM NaCl.

Western blot analysis of these isolated nucleocapsids revealed that they retained the GFP-N1b and GFP-Bd3 fusion proteins and, to a lesser extent, the GFP-N2b fusion protein (Fig. 3A). Notably, this process had stripped almost all M protein from the nucleocapsid (Fig. 3A; compare samples in the second through sixth lanes in the right panel with the sample of the GFP-N1a recombinant in the first lane, for which NP-40 was omitted from the fractionation procedure). The same outcome was obtained at a much higher salt concentration of 250 mM NaCl (Fig. 3B); after such treatment, M protein was undetectable or detectable only in trace amounts, in multiple trials. These results showed that N1b and NBd3, and perhaps N2b, bind directly to the MHV nucleocapsid, either through N-N interactions or through binding to RNA. For the GFP-NBd3 construct, this finding was unexpected. Abundant genetic evidence that NBd3 carries out an essential interaction with the carboxy terminus of the M protein already exists (22, 28, 53, 54). However, the tight binding of GFP-NBd3 to nucleocapsids that were devoid of M protein indicated that the

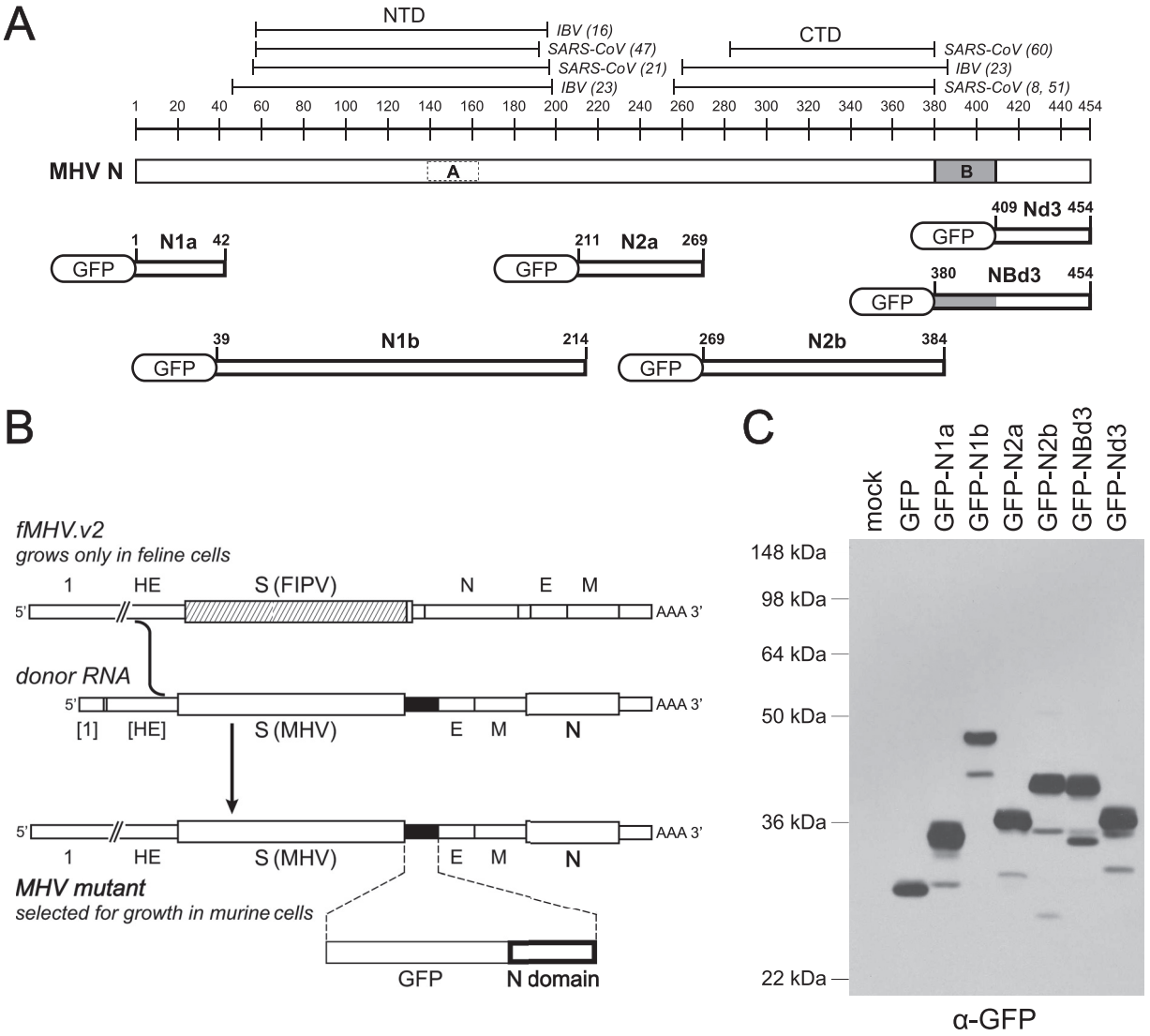

FIG. 1. Construction of MHV recombinants expressing GFP-N-domain fusion proteins. (A) The MHV N protein is represented by a rectangle with three domains separated by two spacers, A and B, as in a previously proposed model (22, 25, 40–42), which has now been partially superseded. The number line indicates amino acid residues. At the top are shown the aligned boundaries of bacterially expressed NTDs and CTDs of the IBV N protein (16, 23) and the SARS-CoV N protein (8, 21, 47, 51, 60) for which X-ray crystal or nuclear magnetic resonance structures have been determined. Beneath the N protein are shown schematics of six GFP fusion constructs that collectively span the length of the MHV N molecule, with N protein amino acid residue numbers given above each construct; GFP moieties are not drawn to scale. (B) Selection of GFP-N-domain expression recombinants by targeted RNA recombination (25, 34). The gene encoding each GFP fusion construct (black rectangle) was inserted into a derivative of transcription vector pMH54 (26) in place of the nonessential gene 4. Donor RNA transcribed from the resulting plasmid was allowed to recombine in infected feline cells with the genome of the interspecies chimera fMHV.v2 (19), which contains the ectodomain-encoding region of the feline infectious peritonitis virus S gene (hatched rectangle) and has a rearrangement of the order of the genes downstream of the S gene. Recombinants were selected on the basis of their ability to grow in murine cells, in contrast to fMHV.v2, which can grow only in feline cells. (C) Western blots of lysates from cells infected with recombinants expressing GFP or GFP-N-domain fusion proteins probed with antibody for GFP. mock, control lysate from mock-infected cells.

Bd3 moiety of N protein additionally participates in some other type of structural interaction.

RNA-binding abilities of GFP-N-domain fusions and other fragments of N protein. To determine whether virion packaging of any of the GFP-N-domain fusion proteins was due to an interaction with RNA, we measured RNA binding by Northwestern assays. Two regions of the viral genome to which the MHV N protein has been reported to exhibit sequence-specific binding are the packaging signal found in the nsp15 coding region of gene 1b (35) and the transcription-regulating sequence found in the leader region of the genome and all subgenomic RNAs (2, 49). Consequently, we used RNA probes encompassing each of these sequences in our assays, and binding was carried out in the presence of an excess of cold competitor cellular RNA. Probe pB1 contained nucleotides 20101 to 20501 of the MHV genome, a region which includes all proposed boundaries of the packaging signal (10, 11, 18, 35, 37). Probe pB36 contained nucleotides 1 to 469 of the genome,

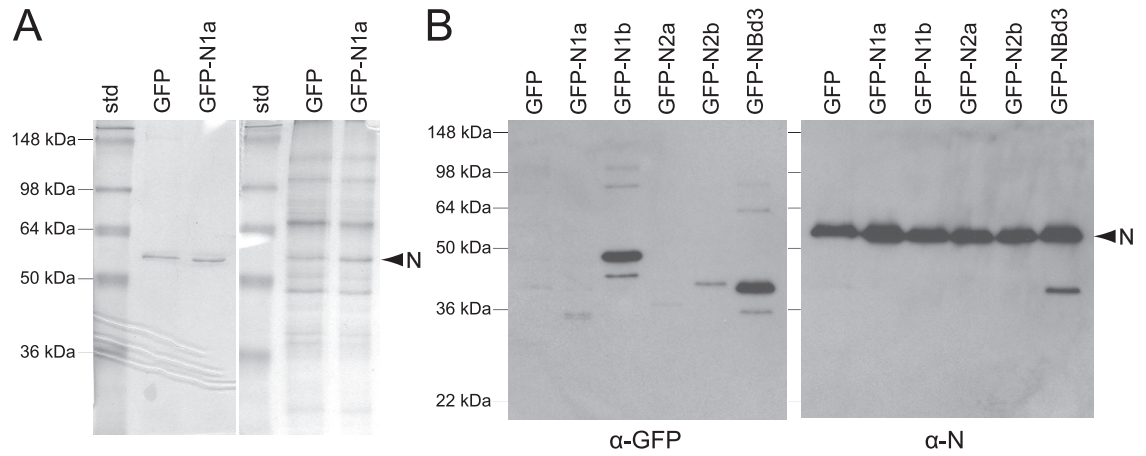

FIG. 2. Incorporation of specific GFP-N-domain fusion proteins into purified MHV virions. (A) Comparison of MHV purification by two rounds of glycerol-tartrate gradients (left panel) or by sucrose flotation (right panel). Equivalent amounts of virions, normalized based on Western blotting with anti-N monoclonal antibody, were separated by SDS-PAGE, and proteins were stained with Coomassie blue. std, molecular mass standard. (B) Western blots of glycerol-tartrate gradient-purified virions probed with antibody for GFP (left panel). The amounts of virions analyzed per lane were normalized such that each lane contained equivalent amounts of N protein, as determined by Western blotting with anti-N monoclonal antibody (right panel).

a region encompassing both the leader and the entire 5′ *cis*-acting element required for RNA replication (24, 33). In blots both of purified virions and of lysates from cells infected with GFP-N-domain recombinants (Fig. 4), labeled pB1 probe RNA was bound by intact viral N protein, but not by any of the GFP-N-domain fusion proteins. The same results were obtained with pB36 probe RNA (data not shown). This finding indicated that the tight association of GFP-N1b, GFP-NBd3, and GFP-N2b with viral nucleocapsids must be due to N protein-N protein interactions and was not due to RNA binding.

To obtain further insight into the participation of different regions of the N protein in RNA binding, we made use of a partially diploid MHV recombinant in which the N gene (and its associated transcription-regulating sequence) is duplicated, replacing the nonessential accessory gene 4 (22) (Fig. 5A). We have previously shown that transposition of the N gene to this upstream position (designated N[2]) results in a completely viable virus (named N transposition-untagged here and MHV-SmNEM in reference 15). Additionally, in another recombinant, named N transposition-tagged, the incorporation of epitope tags into spacer B and at the carboxy terminus of the transposed N gene had little or no effect on viral phenotype. Therefore, in the N duplication-tagged recombinant, the tagged N[2] allele represents a fully functional version of the N gene. Moreover, the tagged version of N[2] protein could be differentiated from its native N[1] counterpart (Fig. 5A).

Starting with the N duplication-tagged recombinant, we constructed a series of 18 in-frame deletions of various sizes, collectively spanning almost the entire N[2] gene (Fig. 5B). All of these deleted N[2] proteins were found to be expressed well in infected cells and were recognized by anti-N antibodies (Fig. 6; data not shown for mutants Δ7 and Δ11). The identities of the deleted N[2] proteins were also confirmed by Western blotting with antibodies against the HA or hexahistidine epitope tags (data not shown). We noted that most of the deleted N proteins, like the full-length N protein, migrated some 4 to 9 kDa more slowly than expected for their predicted molecular masses. The ability of each N[2] deletion mutant to bind to pB1 probe RNA was assessed by Northwestern blotting (Fig. 6). Equivalent results were obtained with pB36 probe RNA (data not shown); moreover, none of the deleted N proteins exhibited a preference for one RNA substrate over the other. As summarized in Fig. 5B, very few of the N[2] protein deletion mutants bound well to RNA. One that did bind well was the Δ20 mutant, in which the carboxy-terminal spacer B and domain 3 of N had been removed; this outcome was consistent with our finding that the GFP-NBd3 fusion protein did not independently bind to MHV RNA. Two other mutants, Δ13 and Δ15, each harboring a small deletion in the N2a region, were also strong RNA binders. In contrast, most of the N protein deletion mutants bound MHV RNA poorly (scored +/−) or not at all (scored −). For the latter group, no signals were detected, even upon very long exposures of autoradiograms such as the ones shown in Fig. 6. Among the nonbinders were deletion mutants in which the complete N1b region (Δ19) or the complete N2b region (Δ3 and Δ4) remained intact. Thus, overall, our data do not support the model of two independent binding sites in the coronavirus N protein that was suggested from studies with bacterially expressed N fragments from SARS-CoV and IBV (6, 8, 16, 21, 51). Instead, our results are more compatible with the notion that the N protein RNA-binding site is bipartite, optimally requiring contributions from both the N1b (NTD) and N2b (CTD) regions of the molecule.

Nonparticipation of spacer B in binding of NBd3 to nucleocapsids. Comprehensive mutagenesis of the 46-amino-acid domain 3 of N protein has uncovered two residues, D440 and D441, that appear to participate in a functionally critical interaction with the carboxy-terminal tail of the M protein (22, 28, 53). However, there has been no prior indication that domain 3 also participates in N-N interactions. To determine whether this latter property actually maps to domain 3 or to the upstream adjacent region, spacer B, we constructed two mutants of spacer B in the GFP-Bd3 fusion protein. Spacer B

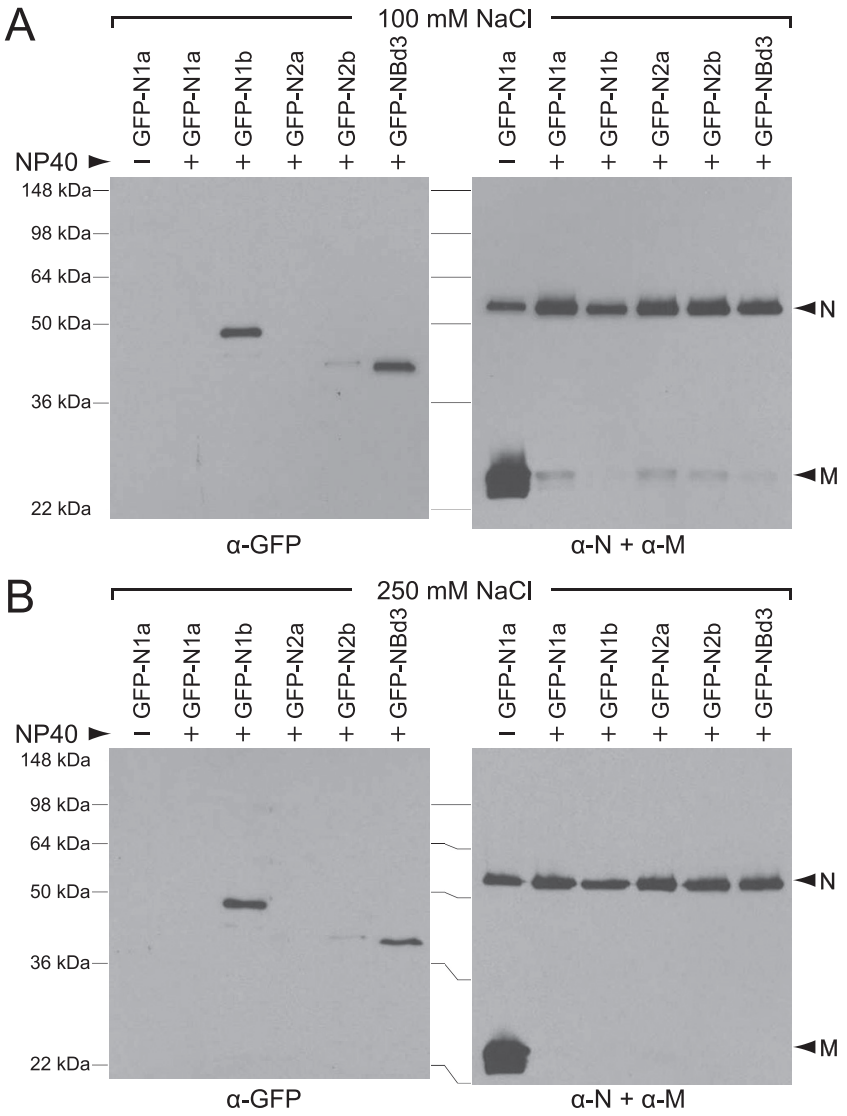

FIG. 3. Fractionation of virions of GFP-N-domain fusion recombinants. Glycerol-tartrate gradient-purified virions were solubilized with 0.25% NP-40 in TME buffer in the presence of either 100 mM NaCl (A) or 250 mM NaCl (B). Samples were pelleted by ultracentrifugation through a step of the same buffer containing 30% glycerol, and half of each pellet was analyzed by use of a Western blot probed either with antibody for GFP (left panels) or with a mixture of anti-N and anti-M monoclonal antibodies (right panels). As a negative control, identical amounts of purified virions of one recombinant, GFP-N1a, were put through the same fractionation procedures in the absence of NP-40 (first lane in each panel).

has been defined as residues 380 to 408 of the MHV N protein (25, 40) (Fig. 7A). In sequence comparisons of many strains of MHV, this segment stands out as the most divergent region within the otherwise highly conserved N protein (40), and it has been shown to tolerate a variety of small substitutions, insertions, and deletions (22, 42). On the other hand, deletion of the entirety of spacer B was found to be the basis for the extreme temperature sensitivity and thermolability of a classical MHV mutant, Alb4 (25). Thus, although we attributed the Alb4 phenotype to the lack of proper spacing between domain 3 and the rest of the N molecule, an additional role for spacer B could not be strictly ruled out.

To replace spacer B with a heterologous sequence of equal size, we designed a flexible linker of multiple glycines with interspersed serines and threonines, based on structural principles established for engineered proteins (45). Additionally, we inserted a protease cleavage site in the center of the linker, for potential future use. In the resulting mutant, designated GFP-NBd3-PR, 26 of the 29 residues of spacer B were thereby changed (Fig. 7A). Lysates from cells infected with the GFP-NBd3-PR recombinant expressed the mutant fusion protein in amounts comparable to those produced by the GFP-NBd3 recombinant (Fig. 7B). The slightly higher mobility in SDS-PAGE of the GFP-NBd3-PR fusion protein than of GFP-NBd3 was likely due to the reduced molecular mass of the mutant, resulting from the many glycine substitutions for larger residues. We also constructed a second mutant, GFP-NBd3-CCA, in which 9 of 13 charged residues in spacer B were replaced by alanines (Fig. 7A). However, two independent recombinants containing exactly the intended sequence failed

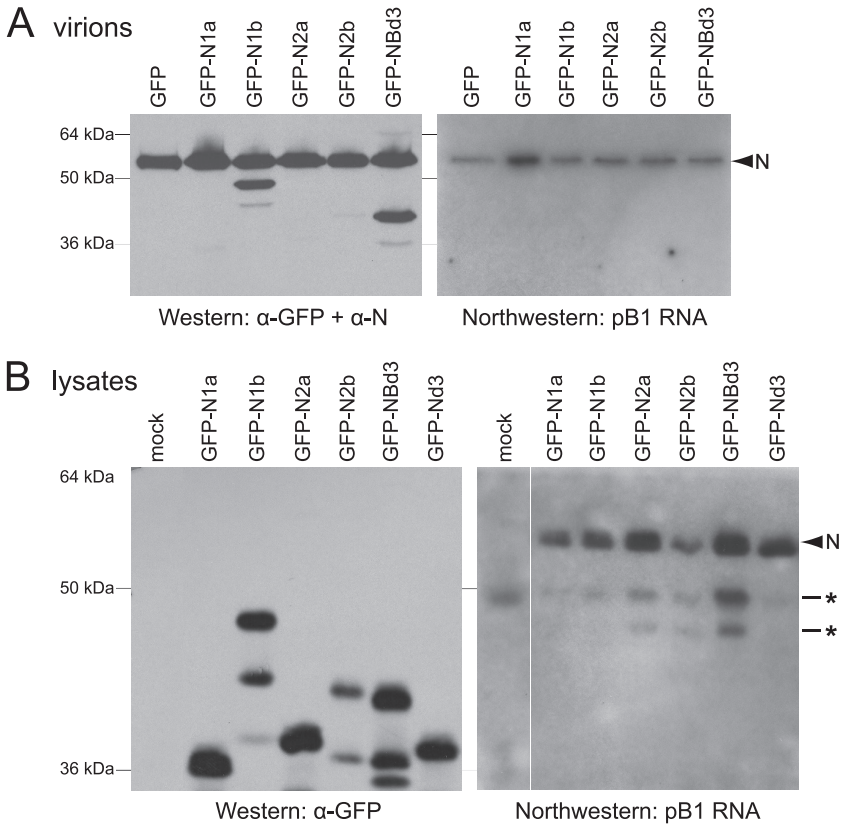

FIG. 4. RNA binding by GFP-N-domain fusion proteins. Purified virions (A) or lysates from cells infected with recombinants expressing GFP-N-domain fusion proteins (B) were analyzed by use of Northwestern blots (right panels) probed with pB1 RNA, which corresponds to the region of the MHV genome containing the packaging signal (10, 11, 18, 35, 37). Asterisks denote nonspecific bands due either to cellular proteins or to proteolytic products of full-length N protein. A duplicate of each set of samples was analyzed by use of a Western blot (left panels) probed either with antibody for GFP (B) or with a mixture of anti-GFP and anti-N monoclonal antibodies (A). mock, control lysate from mock-infected cells.

to express detectable levels of the mutant GFP fusion protein. A third recombinant, GFP-NBd3-CCA*, was able to express the mutant fusion protein, but it was shown to have an altered sequence in which the AAAAA substitutions replacing spacer B residues 402 to 406 had changed to APAAA. From these findings, we concluded that the multiple spacer B charged-to-alanine mutations had unanticipated effects on GFP-NBd3 folding and degradation; we therefore deemed the GFP-NBd3-CCA mutant to not be suitable for further analysis.

Like its wild-type counterpart, the GFP-NBd3-PR fusion protein was incorporated into purified virions (Fig. 7C). Moreover, GFP-NBd3-PR remained stably associated with the viral nucleocapsid following NP-40 solubilization of viruses in the presence of 100 mM or 250 mM NaCl (Fig. 7D), in the same manner as did GFP-NBd3. Under the latter conditions, M protein was almost completely removed from the nucleocapsid. This demonstrated that, in assembled virions, domain 3 of the N protein participates in a tight N-N interaction, to which spacer B makes no substantial contribution. This result agrees well with results from a previous study, in which the Alb4 mutant N protein was shown to be fully competent, at the permissive temperature, in formation of a stable homotypic N protein interaction in the virion nucleocapsid (36).

In order to test directly the functionality of the completely heterologous linker in GFP-NBd3-PR, we constructed the identical spacer B replacement in the native N gene of MHV, in an otherwise wild-type background. The engineered viral mutant was obtained at a high frequency by targeted RNA recombination, and it formed only slightly smaller plaques than did wild-type virus (data not shown). This result strongly indicated that, as originally suggested (40), spacer B is an essentially inert linker that serves only to tether domain 3 to the rest of the N molecule at an appropriate distance.

Mutational disruption of the binding of domain N1b to nucleocapsids. To begin to explore the N-N interaction in which domain N1b participates, we created a set of mutants of the GFP-N1b recombinant. Our strategy was to mutate surface clusters of charged residues in MHV domain N1b, informed by inspection of the highly similar crystal structures that have been determined for the aligned NTDs of the IBV and SARS-CoV N proteins (16, 47). On this basis, we constructed charged-to-alanine mutations at three loci (Fig. 8A). mut1 and mut3 altered patches on opposite surfaces surrounding the main core of the NTD, which is a five-stranded antiparallel beta sheet; mut2 fell within a beta-hairpin turn that protrudes from the main mass of the structure. Recombinants encoding all three mutant fusions were isolated, but the GFP-N1b-mut1 recombinant was found to express little or no detectable GFP

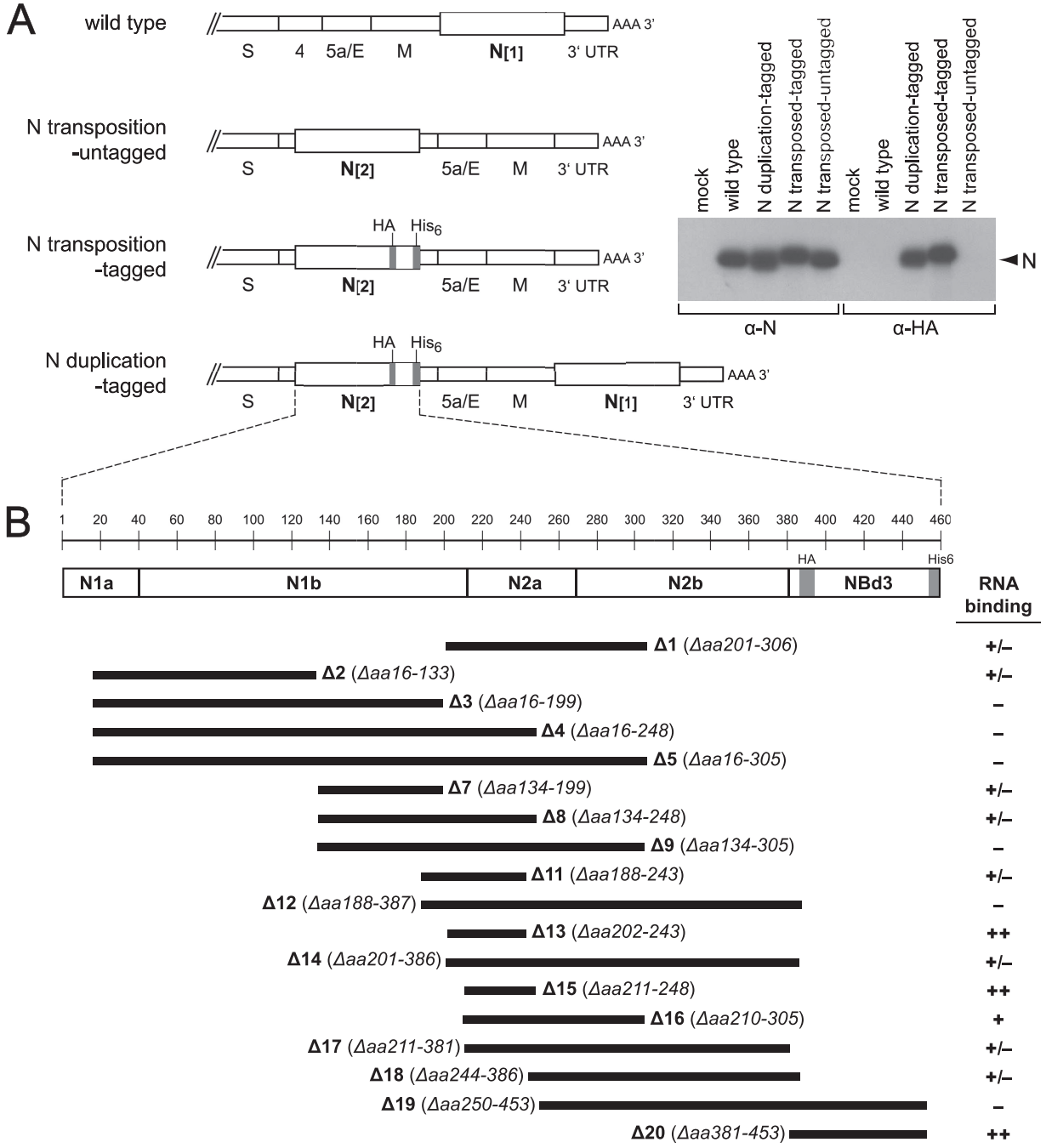

FIG. 5. RNA binding by MHV N protein deletion mutants expressed from a duplicated N gene. (A) Schematic of the downstream end of the genome for wild-type MHV and for three recombinants in which the N gene is transposed or duplicated. For each, the wild-type copy of the N gene, in its normal genomic locus, is designated N[1] and the transposed or duplicated copy of the N gene is designated N[2]. In the N transposition-untagged recombinant, the N[2] gene is identical to the wild-type N gene. In the N transposition-tagged and the N duplication-tagged recombinants, the N[2] gene has been labeled with HA and His_6 epitope tags, indicated by gray rectangles. The inset at the right shows N protein from lysates of [^{35}S]methionine-labeled infected cells or uninfected cells (mock) immunoprecipitated with either anti-N polyclonal antibody or anti-HA monoclonal antibody. (B) Expansion of the schematic of the N[2] gene in the N duplication-tagged recombinant. The number line indicates amino acid residues, and the boundaries of the N1a, N1b, N2a, N2b, and NBd3 regions are represented. The HA epitope tag replaces amino acids 386 to 394 of spacer B; the His_6 epitope tag is appended to the carboxy terminus of the N molecule. Beneath are shown the loci of the N[2] deletions in 18 separate mutants of the N duplication-tagged recombinant. The RNA-binding ability of each N protein deletion mutant is summarized at the right.

fusion protein (Fig. 8B). Consistent with this failure of expression, when the three amino acid mutations of mut1 were incorporated into the native N gene, in an otherwise wild-type background, the mutant that was generated formed small plaques and was temperature sensitive and thermolabile. Interestingly, multiple independent large-plaque revertants of the native N-mut1 virus all were found to have acquired a second-site reverting mutation, Q187K (Fig. 8A); the counter-

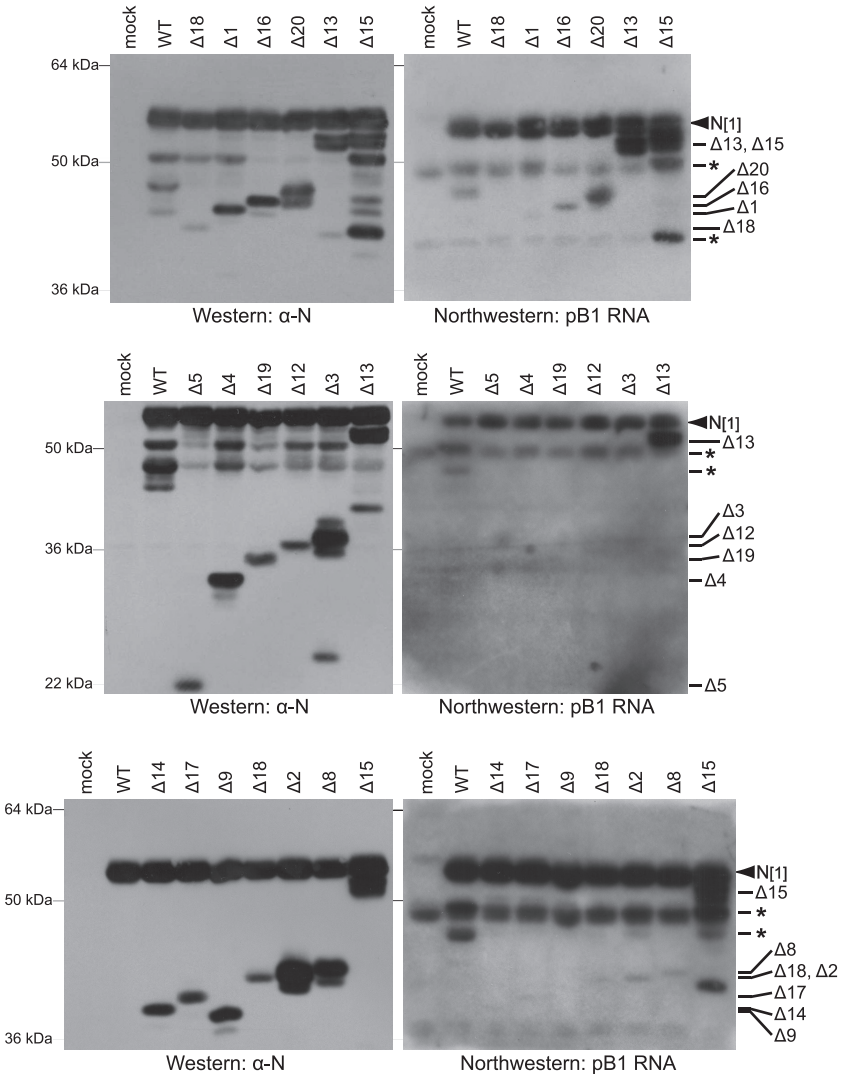

FIG. 6. RNA binding by N protein duplication-deletion mutants. Lysates from cells infected with deletion mutants of the N duplication-tagged recombinant (Fig. 5B) were analyzed by use of Northwestern blots (right panels) probed with pB1 RNA, which corresponds to the region of the MHV genome containing the packaging signal (10, 11, 18, 35, 37). Asterisks denote nonspecific bands due either to cellular proteins or to proteolytic products of full-length N protein. A duplicate of each set of samples was analyzed by use of a Western blot (left panels) probed either with anti-N polyclonal antibody (top and middle panels) or monoclonal antibody (bottom panel). mock, control lysate from mock-infected cells; WT, N duplication-tagged recombinant with no deletion in the N[2] gene.

part of this residue falls very close to the locus of the primary mutations of mut1 in the SARS-CoV NTD structure (47). The characteristics of the native N-mut1 virus and its revertants suggested that the mutations in GFP-N1b-mut1 caused a general aberration in GFP-N1b folding, leading to degradation of the fusion protein. Therefore, the mut1 constructs did not implicate specific residues as being involved in the domain N1b interaction with the viral nucleocapsid.

The GFP-N1b-mut2 and GFP-N1b-mut3 recombinants expressed their respective mutant GFP fusion proteins well in infected cells, although not as abundantly as did the wild-type GFP-N1b recombinant (Fig. 8B). Notably, however, only very small quantities of either of these mutant GFP fusion proteins became incorporated into virions (data not shown). Moreover, absolutely no detectable amount of either the GFP-N1b-mut2 or the GFP-N1b-mut3 fusion protein remained associated with viral nucleocapsids following virion solubilization with NP-40 in the presence of 100 mM NaCl (Fig. 8C) or 250 mM NaCl (data not shown). Thus, the mut2 and mut3 mutations effectively disrupted the interaction of domain N1b with N protein.

We carried out multiple independent targeted RNA recombination experiments to introduce the four amino acid mutations of mut3 into the native N gene of MHV. Nevertheless, all such attempts had negative outcomes, despite parallel positive controls with wild-type donor RNA that yielded robust frequencies of recombinants. By this latter criterion, we inferred that the mut3 lesion is lethal in native N protein. Similarly, native N protein was refractory to acceptance of the three amino acid mutations of mut2. Following multiple attempts, we obtained only one recombinant, which produced smaller plaques than the wild type. This recombinant contained the unintended mutation K120V, rather than K120A, constituting

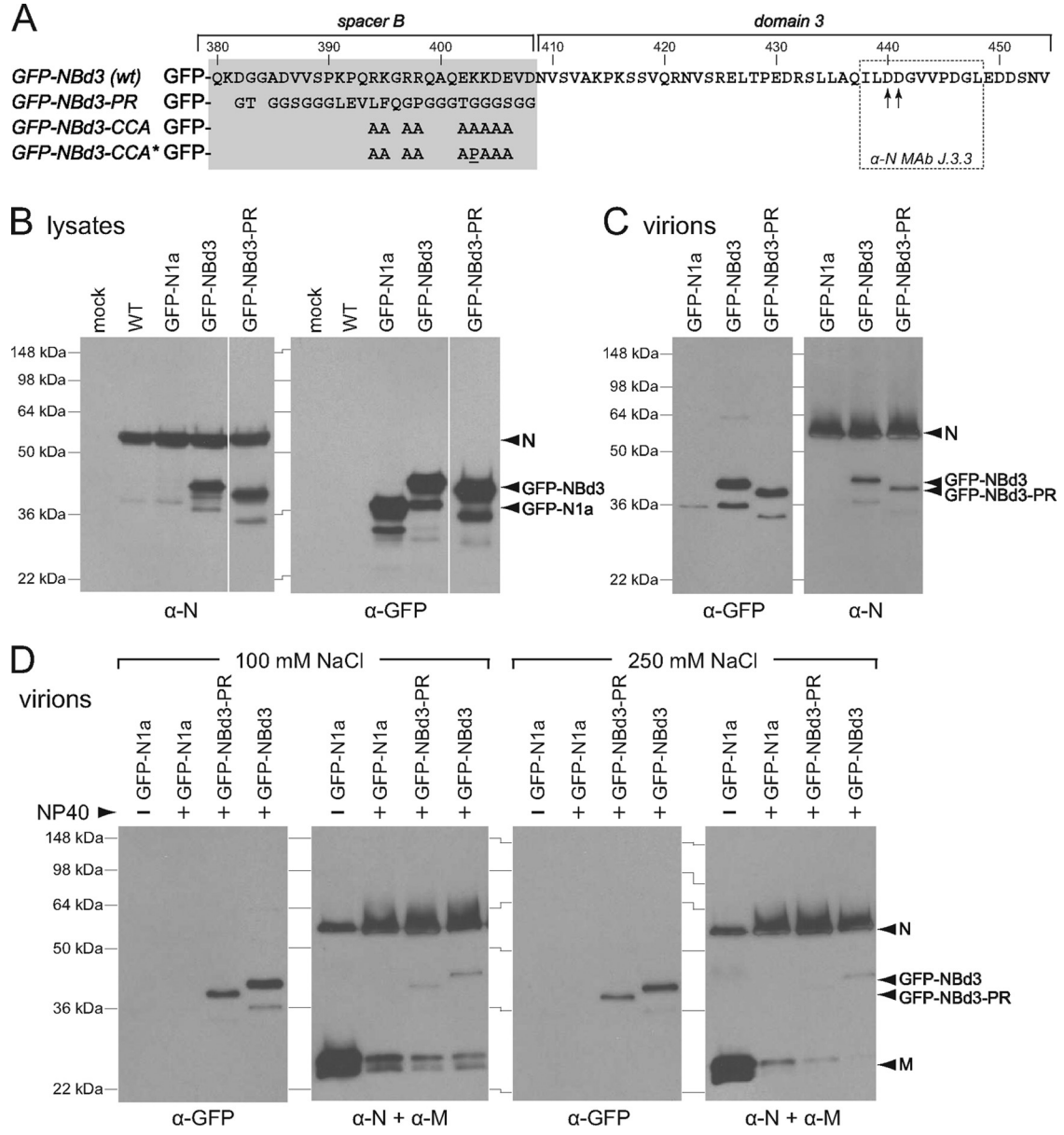

FIG. 7. Mutation of spacer B of the N protein. (A) Schematic of GFP-NBd3 mutants. The sequence of the spacer B (shaded rectangle) and domain 3 portion of the GFP-NBd3 fusion protein is given in the top line. This sequence is identical to that of the carboxy terminus of the wild-type N protein, starting at amino acid 380; residue numbers correspond to those of the native N protein. For the mutants GFP-NBd3-PR, GFP-NBd3-CCA, and GFP-NBd3-CCA*, only residues that differ from the wild type are shown. Also depicted are the previously mapped epitope for anti-N monoclonal antibody J.3.3 (dotted rectangle) and two aspartate residues critical for interaction between the N and M proteins (arrows) (22). (B) Western blots of lysates from cells infected with recombinants expressing GFP-N-domain fusion proteins probed either with antibody for GFP (right panel) or with anti-N monoclonal antibody (left panel). Lysates from mock-infected or wild-type (WT)-infected cells are shown as controls. (C) Incorporation of GFP-NBd3-PR mutant protein into purified MHV virions. Western blots of glycerol-tartrate gradient-purified virions were probed with antibody for GFP (left panel). The amounts of virions analyzed in each lane were normalized so as to contain equivalent amounts of N protein, as determined by Western blotting with anti-N monoclonal antibody (right panel). (D) Fractionation of virions of the GFP-NBd3-PR mutant. Glycerol-tartrate gradient-purified virions were solubilized with 0.25% NP-40 in TME buffer in the presence of either 100 mM NaCl (left panels) or 250 mM NaCl (right panels). Samples were pelleted by ultracentrifugation through a step of the same buffer containing 30% glycerol, and half of each pellet was analyzed by use of a Western blot probed either with antibody for GFP (first and third panels) or with a mixture of anti-N and anti-M monoclonal antibodies (second and fourth panels). As a negative control, identical amounts of purified virions of the GFP-N1a recombinant were subjected to the same fractionation procedures in the absence of NP-40 (first lane in each panel).

a variant of mut2 that we designated mut2* (Fig. 8A). When the mut2* mutations were then reconstructed in a GFP-N1b recombinant, the resulting GFP-N1b-mut2* fusion protein was expressed to the same extent as was the GFP-N1b-mut2 fusion protein (Fig. 8B). However, the GFP-N1b-mut2* fusion protein was also unable to stably associate with nucleocapsids fractionated from purified virions (Fig. 8C). Thus, the mut2* mutations constitute a lesion that is partially defective in native

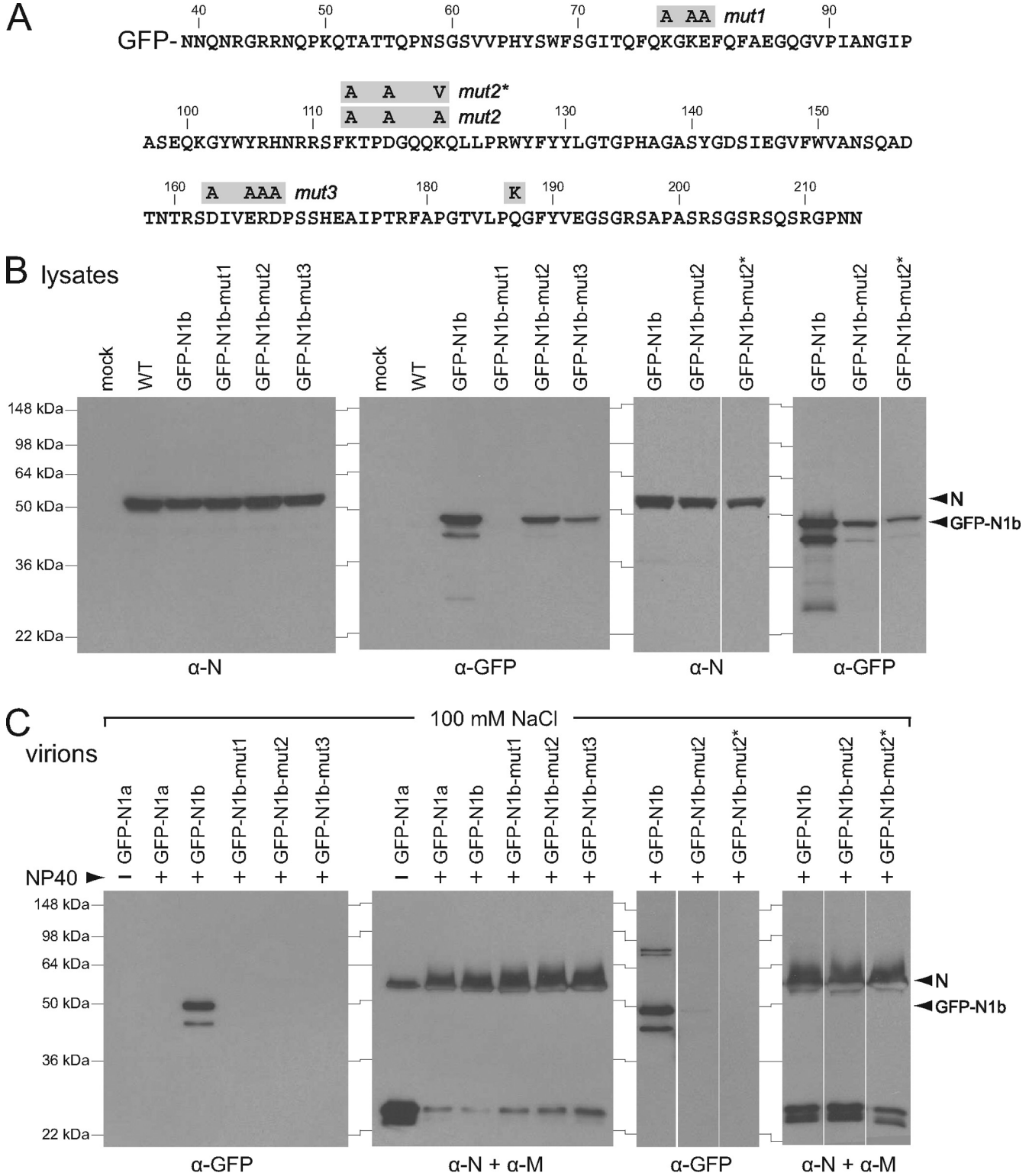

FIG. 8. Mutation of domain 1b of the N protein. (A) Schematic of GFP-N1b mutants. The sequence of the domain 1b portion of the GFP-N1b fusion protein, comprising amino acids 39 through 214 of the wild-type N protein sequence, is shown. The mutated residues of GFP-N1b-mut1, -mut2, -mut2*, and -mut3 are indicated in shaded boxes above the sequence. Also shaded is the Q187 mutation found in second-site revertants of mut1 constructed in the native N gene. (B) Western blots of lysates from cells infected with recombinants expressing GFP-N1b fusion protein or mutants probed either with antibody for GFP (second and fourth panels) or with anti-N monoclonal antibody (first and third panels). Lysates from mock-infected and wild-type (WT)-infected cells are shown as controls. (C) Fractionation of virions of the GFP-N1b recombinant and mutants. Glycerol-tartrate gradient-purified virions were solubilized with 0.25% NP-40 in TME buffer in the presence of 100 mM NaCl. Samples were pelleted by ultracentrifugation through a step of the same buffer containing 30% glycerol, and half of each pellet was analyzed by use of a Western blot probed either with antibody for GFP (first and third panels) or with a mixture of anti-N and anti-M monoclonal antibodies (second and fourth panels). As a negative control, identical amounts of purified virions of the GFP-N1a recombinant were subjected to the same fractionation procedures in the absence of NP-40 (first lane in first and second panels).

N protein and completely defective in the GFP-N1b construct. Taken together, the results with mut2 and mut3 suggest that the N-N interaction of domain N1b is important, and possibly essential, for viral viability.

DISCUSSION

In this study, we examined in vivo assembly interactions of different domains of the MHV N protein, each of which was expressed as a GFP fusion protein during the course of viral infection. We found that fusion constructs containing two of the N domains, N1b and NBd3, were incorporated into assembled virions. Virion fractionation procedures showed that incorporation of either of these two fusion proteins was due to its tight association with the viral nucleocapsid, which is a complex of the N protein and genomic RNA. Nucleocapsid binding by GFP-N1b or GFP-NBd3 was stable in the presence of as much as 250 mM NaCl and was sufficiently strong to withstand the forces generated by ultracentrifugation. Under the same conditions, essentially all M protein was released from association with the nucleocapsid. Northwestern blot analyses indicated that the N1b and NBd3 domains were not capable of independently binding to RNA. We therefore concluded that N protein-N protein interactions were the basis for the persistent association of each of these two separate domains with the viral nucleocapsid. For the GFP-NBd3 construct, we further showed that the tight N-N interaction is mediated by domain 3 of the N protein, given that the spacer B segment of this fusion protein could be replaced by an entirely heterologous peptide segment of the same size. For the GFP-N1b construct, we identified two regions of the surface of the N1b domain, those defined by the residues altered in mut2 and in mut3, that affected the tight N-N interaction in which the N1b domain participates.

Our division of the MHV N protein into separate domains was guided in large part by results from a number of recent structural and biophysical studies of the SARS-CoV and IBV N proteins. These studies, all utilizing bacterially expressed protein fragments, have found two independently folding coronavirus N protein segments, the NTD and the CTD (corresponding to our domains N1b and N2b [Fig. 1]), for which nuclear magnetic resonance or X-ray crystal structures have been determined (8, 16, 21, 23, 47, 51, 60). The remainder of the N molecule—the amino terminus, the central linker containing the SR-rich region, and the carboxy terminus (corresponding to our domains N1a, N2a, and NBd3, respectively)—appears to consist of polypeptides that are intrinsically disordered, at least in the absence of the RNA or protein molecules to which they bind (6, 7). Both the NTD and the CTD have been shown to separately possess RNA-binding ability (6, 8, 16, 21, 30, 51, 59, 61). N protein-N protein association, on the other hand, is generally seen as a property of the CTD, which is sometimes designated the dimerization domain (7, 16, 23, 60). Under some conditions, the CTD has been found to multimerize into tetramers and octamers, but the significance of this capability is unclear (8, 30, 51, 59). The NTD of the IBV N protein also has a weak propensity for dimerization (16, 23). Further, it has been claimed that SARS-CoV N protein self-association is governed by the SR-rich region of that protein (31).

Our findings in the present work contrast somewhat with the evolving modular model of the coronavirus N protein. We might have expected virion incorporation of the GFP-N1b fusion protein (containing the MHV counterpart of the NTD) to be mediated by N1b binding to genomic RNA. However, we did not detect RNA binding by GFP-N1b or by any of the other GFP-N domain fusion proteins, under conditions where very strong RNA binding by native N protein occurred (Fig. 4). Moreover, our analysis of a collection of MHV N protein deletion mutants showed that only domain Bd3 and the SR-rich portion of domain 2a were clearly dispensable for RNA-binding ability (Fig. 5 and 6). Our results suggested that RNA binding by the N protein requires contributions from both the NTD and the CTD; thus, the separately expressed N1b domain could not compete with native N protein for RNA binding within the nucleocapsid. Three significant properties of our Northwestern assays should be noted: (i) they were performed using RNA substrates to which the MHV N protein has been shown to bind in a sequence-specific manner (2, 35, 49); (ii) RNA binding was carried out in the presence of a large molar excess of unlabeled competitor RNA; and (iii) N proteins, fusion proteins, and deletion mutants were produced under conditions of viral infection in eukaryotic cells and were therefore expected to be subject to phosphorylation (5, 9, 43, 55) and any other modifications normally carried by N. In contrast, most of the binding assays that have been performed with bacterially expressed NTD and CTD constructs employed nonspecific RNA (or DNA) substrates in the absence of competitor nucleic acids (6, 8, 16, 21, 30, 59). Thus, the interactions measured by these investigations were apparently too weak to have been detected in our assays. In accord with our results, however, a recent study of the SARS-CoV N protein found that a bacterially expressed construct containing both the NTD and CTD displayed an affinity for a nonspecific RNA substrate greater than 10-fold higher than that of either the NTD or the CTD alone (6).

With respect to N protein-N protein interactions, we might have expected the GFP-N2b fusion protein (containing the MHV counterpart of the CTD) to exhibit the strongest binding to the nucleocapsid. However, the level of incorporation of this construct into assembled virions was minimal, compared to that for the GFP-N1b and GFP-Bd3 fusion proteins. This observation may mean that the separate GFP-N2b protein cannot effectively compete with CTD-CTD interactions among native N proteins within the intact nucleocapsid. Even for the more efficiently packaged GFP fusion proteins, the overall stoichiometry of virion incorporation with respect to the native N protein appeared to be low. This can be inferred from a comparison of the relative amounts of the N and GFP-NBd3 proteins in the second Western blot in Fig. 2B, which was probed with an anti-N monoclonal antibody that recognizes the same domain 3 epitope in each protein (Fig. 7A). Thus, although we believe that the selective packaging of three of the GFP-N-domain fusion proteins resulted from their appropriation of some subset of normal N-N interactions, such substitution was limited by the monovalent nature of the fusion proteins and their inability to bind RNA. In contrast, native N monomers, each containing the full complement of domains, could interact cooperatively and with higher avidity within the assembled nucleocapsid. The ineffective competitive potential of the

abundantly expressed GFP-N-domain fusion proteins would also explain why none of them exhibited an observable dominant-negative effect on MHV. Recombinants expressing the fusion proteins were not noticeably impaired with respect to the wild type and remained stable for multiple passages. It is therefore notable that significant instability was observed in a dual recombinant that paired the GFP-NBd3 gene with a native N gene containing the domain 1b mut2* mutations. In multiple independent isolates of this mutant, the GFP-NBd3 gene was rapidly lost through deletion, presumably because, in this case, the fusion protein was better able to disrupt the impaired interactions between monomers of the mutant N protein (K. Hurst and P. Masters, unpublished data).

We do not yet know if our separately observed associations of the N1b and NBd3 domains with the MHV nucleocapsid are indicative of two symmetric interactions, namely, N1b-N1b and NBd3-NBd3. Alternatively, they could represent reciprocal aspects of a single head-to-tail interaction, N1b-NBd3. We are currently attempting to discriminate between these two possibilities. A more complete understanding of the nature of the N1b and NBd3 interactions and nucleocapsid assembly will also need to address other matters, including (i) whether a given type of interaction occurs between adjacent monomers on the RNA strand or, instead, connects nonadjacent monomers at each helical turn; (ii) how densely N protein monomers are distributed per length of RNA; and (iii) to what extent the different crystal packing arrangements from the NTD and CTD structural determinations (8, 23, 47) reflect the organization of the viral nucleocapsid.

A further complexity is how to reconcile the tight NBd3-nucleocapsid interaction with the previously established NBd3-M protein interaction, which was discovered by genetic means (22, 28, 53). One potential explanation is that NBd3 docks with the carboxy terminus of the M protein in order to initiate budding but is then handed over to its N-domain partner (N1b or another NBd3 moiety) in order to stabilize the higher-order structure of the packaged nucleocapsid. However, this scenario seems less plausible in light of the astonishing structural details revealed by recent cryo-electron microscopic (38) and cryo-electron tomographic (1) studies of MHV and other coronaviruses. Both of these studies have shown thread-like connections between the M protein endodomain and the nucleocapsid within virions, suggesting that the NBd3-M protein interaction persists, even after assembly is completed. Therefore, based on currently available information, a more likely model is that domain 3 of each N protein monomer is engaged in only one of two alternative modes of binding in the assembled virion, either with another N monomer or with the carboxy terminus of an M molecule in the virion envelope. It is not yet clear whether the interactions of NBd3 with the N and M proteins, respectively, involve two separable segments of domain 3 or if they are multiple functions of the same segment. Genetic analyses of domain 3 to date, although comprehensively covering the whole domain, have found only a single locus, residues D440 and D441, which appears critical for N-M interactions (22, 53). It remains to be determined whether mutations at this site also affect N-N interactions or if it will be possible to genetically differentiate between N-N and N-M interactions. As an alternative approach, further work with the native N protein NBd3-PR mutant may allow us to define more precisely the interactions of N protein domain 3 with its binding partners in assembled virions.

ACKNOWLEDGMENTS

We are grateful to John Fleming (University of Wisconsin—Madison) for generously providing monoclonal antibodies J.3.3 and J.1.3 and to Scott Goebel for the construction of some plasmids. We thank the Applied Genomics Technology Core Facility of the Wadsworth Center for DNA sequencing.

This work was supported by Public Health Service grant AI 64603 from the National Institutes of Health.

REFERENCES

1. **Bárcena, M., G. T. Oostergetel, W. Bartelink, F. G. A. Faas, A. Verkleij, P. J. M. Rottier, A. J. Koster, and B. J. Bosch.** 2009. Cryo-electron tomography of mouse hepatitis virus: insights into the structure of the coronavirion. Proc. Natl. Acad. Sci. USA **106:**582–587.
2. **Baric, R. S., G. W. Nelson, J. O. Fleming, R. J. Deans, J. G. Keck, N. Casteel, and S. A. Stohlman.** 1988. Interactions between coronavirus nucleocapsid protein and viral RNAs: implications for viral transcription. J. Virol. **62:** 4280–4287.
3. **Block, K. L., H. P. Vornlocher, and J. W. Hershey.** 1998. Characterization of cDNAs encoding the p44 and p35 subunits of human translation initiation factor eIF3. J. Biol. Chem. **273:**31901–31908.
4. **Boscarino, J. A., H. L. Logan, J. J. Lacny, and T. M. Gallagher.** 2008. Envelope protein palmitoylations are crucial for murine coronavirus assembly. J. Virol. **82:**2989–2999.
5. **Calvo, E., D. Escors, J. A. Lopez, J. M. Gonzalez, A. Alvarez, E. Arza, and L. Enjuanes.** 2005. Phosphorylation and subcellular localization of transmissible gastroenteritis virus nucleocapsid protein in infected cells. J. Gen. Virol. **86:**2255–2267.
6. **Chang, C.-K., Y.-L. Hsu, Y.-H. Chang, F.-A. Chao, M.-C. Wu, Y.-S. Huang, C.-K. Hu, and T.-H. Huang.** 2009. Multiple nucleic acid binding sites and intrinsic disorder of severe acute respiratory syndrome coronavirus nucleocapsid protein: implications for ribonucleocapsid protein packaging. J. Virol. **83:**2255–2264.
7. **Chang, C.-K., S.-C. Sue, T.-H. Yu, C.-M. Hsieh, C.-K. Tsai, Y.-C. Chiang, S.-J. Lee, H.-H. Hsiao, W.-J. Wu, W.-L. Chang, C.-H. Lin, and T.-H. Huang.** 2006. Modular organization of SARS coronavirus nucleocapsid protein. J. Biomed. Sci. **13:**59–72.
8. **Chen, C.-Y., C.-K. Chang, Y.-W. Chang, S.-C. Sue, H.-I. Bai, L. Riang, C.-D. Hsiao, and T.-H. Huang.** 2007. Structure of the SARS coronavirus nucleocapsid protein RNA-binding dimerization domain suggests a mechanism for helical packaging of viral RNA. J. Mol. Biol. **368:**1075–1086.
9. **Chen, H., A. Gill, B. K. Dove, S. R. Emmett, C. F. Kemp, M. A. Ritchie, M. Dee, and J. A. Hiscox.** 2005. Mass spectroscopic characterization of the coronavirus infectious bronchitis virus nucleoprotein and elucidation of the role of phosphorylation in RNA binding by using surface plasmon resonance. J. Virol. **79:**1164–1179.
10. **Chen, S. C., E. van den Born, S. H. van den Worm, C. W. Pleij, E. J. Snijder, and R. C. Olsthoorn.** 2007. New structure model for the packaging signal in the genome of group IIa coronaviruses. J. Virol. **81:**6771–6774.
11. **Cologna, R., and B. G. Hogue.** 2000. Identification of a bovine coronavirus packaging signal. J. Virol. **74:**580–583.
12. **Das Sarma, J., E. Scheen, S. H. Seo, M. Koval, and S. R. Weiss.** 2002. Enhanced green fluorescent protein expression may be used to monitor murine coronavirus spread in vitro and in the mouse central nervous system. J. Neurovirol. **8:**381–391.
13. **de Haan, C. A. M., P. S. Masters, X. Shen, S. Weiss, and P. J. M. Rottier.** 2002. The group-specific murine coronavirus genes are not essential, but their deletion, by reverse genetics, is attenuating in the natural host. Virology **296:**177–189.
14. **de Haan, C. A. M., and P. J. M. Rottier.** 2005. Molecular interactions in the assembly of coronaviruses. Adv. Virus Res. **64:**165–230.
15. **de Haan, C. A. M., H. Volders, C. A. Koetzner, P. S. Masters, and P. J. M. Rottier.** 2002. Coronaviruses maintain viability despite dramatic rearrangements of the strictly conserved genome organization. J. Virol. **76:**12491–12493.
16. **Fan, H., A. Ooi, Y. W. Tan, S. Wang, S. Fang, D. X. Liu, and J. Lescar.** 2005. The nucleocapsid protein of coronavirus infectious bronchitis virus: crystal structure of its N-terminal domain and multimerization properties. Structure **13:**1859–1868.
17. **Fischer, F., C. F. Stegen, C. A. Koetzner, and P. S. Masters.** 1997. Analysis of a recombinant mouse hepatitis virus expressing a foreign gene reveals a novel aspect of coronavirus transcription. J. Virol. **71:**5148–5160.
18. **Fosmire, J. A., K. Hwang, and S. Makino.** 1992. Identification and characterization of a coronavirus packaging signal. J. Virol. **66:**3522–3530.

19. **Goebel, S. J., B. Hsue, T. F. Dombrowski, and P. S. Masters.** 2004. Characterization of the RNA components of a putative molecular switch in the 3′ untranslated region of the murine coronavirus genome. J. Virol. **78:**669–682.
20. **Horton, R. M., and L. R. Pease.** 1991. Recombination and mutagenesis of DNA sequences using PCR. p. 217–247. *In* M. J. McPherson (ed.), Directed mutagenesis, a practical approach. IRL Press, New York, NY.
21. **Huang, Q., L. Yu, A. M. Petros, A. Gunasekera, Z. Liu, N. Xu, P. Hajduk, J. Mack, S. W. Fesik, and E. T. Olejniczak.** 2004. Structure of the N-terminal RNA-binding domain of the SARS CoV nucleocapsid protein. Biochemistry **43:**6059–6063.
22. **Hurst, K. R., L. Kuo, C. A. Koetzner, R. Ye, B. Hsue, and P. S. Masters.** 2005. A major determinant for membrane protein interaction localizes to the carboxy-terminal domain of the mouse coronavirus nucleocapsid protein. J. Virol. **79:**13285–13297.
23. **Jayaram, H., H. Fan, B. R. Bowman, A. Ooi, J. Jayaram, E. W. Collisson, J. Lescar, and B. V. Prasad.** 2006. X-ray structures of the N- and C-terminal domains of a coronavirus nucleocapsid protein: implications for nucleocapsid formation. J. Virol. **80:**6612–6620.
24. **Kim, Y.-N., Y. S. Jeong, and S. Makino.** 1993. Analysis of *cis*-acting sequences essential for coronavirus defective interfering RNA replication. Virology **197:**53–63.
25. **Koetzner, C. A., M. M. Parker, C. S. Ricard, L. S. Sturman, and P. S. Masters.** 1992. Repair and mutagenesis of the genome of a deletion mutant of the coronavirus mouse hepatitis virus by targeted RNA recombination. J. Virol. **66:**1841–1848.
26. **Kuo, L., G.-J. Godeke, M. J. B. Raamsman, P. S. Masters, and P. J. M. Rottier.** 2000. Retargeting of coronavirus by substitution of the spike glycoprotein ectodomain: crossing the host cell species barrier. J. Virol. **74:**1393–1406.
27. **Kuo, L., K. R. Hurst, and P. S. Masters.** 2007. Exceptional flexibility in the sequence requirements for coronavirus small envelope protein function. J. Virol. **81:**2249–2262.
28. **Kuo, L., and P. S. Masters.** 2002. Genetic evidence for a structural interaction between the carboxy termini of the membrane and nucleocapsid proteins of mouse hepatitis virus. J. Virol. **76:**4987–4999.
29. **Laude, H., and P. S. Masters.** 1995. The coronavirus nucleocapsid protein, p. 141–163. *In* S. G. Siddell (ed.), The Coronaviridae. Plenum Press, New York, NY.
30. **Luo, H., J. Chen, K. Chen, X. Shen, and H. Jiang.** 2006. Carboxyl terminus of severe acute respiratory syndrome coronavirus nucleocapsid protein: self-association analysis and nucleic acid binding characterization. Biochemistry **45:**11827–11835.
31. **Luo, H., F. Ye, K. Chen, X. Shen, and H. Jiang.** 2005. SR-rich motif plays a pivotal role in recombinant SARS coronavirus nucleocapsid protein multimerization. Biochemistry **44:**15351–15358.
32. **Masters, P. S.** 2006. The molecular biology of coronaviruses. Adv. Virus Res. **66:**193–292.
33. **Masters, P. S., C. A. Koetzner, C. A. Kerr, and Y. Heo.** 1994. Optimization of targeted RNA recombination and mapping of a novel nucleocapsid gene mutation in the coronavirus mouse hepatitis virus. J. Virol. **68:**328–337.
34. **Masters, P. S., and P. J. M. Rottier.** 2005. Coronavirus reverse genetics by targeted RNA recombination. Curr. Top. Microbiol. Immunol. **287:**133–159.
35. **Molenkamp, R., and W. J. M. Spaan.** 1997. Identification of a specific interaction between the coronavirus mouse hepatitis virus A59 nucleocapsid protein and packaging signal. Virology **239:**78–86.
36. **Narayanan, K., K. H. Kim, and S. Makino.** 2003. Characterization of N protein self-association in coronavirus ribonucleoprotein complexes. Virus Res. **98:**131–140.
37. **Narayanan, K., and S. Makino.** 2001. Cooperation of an RNA packaging signal and a viral envelope protein in coronavirus RNA packaging. J. Virol. **75:**9059–9067.
38. **Neuman, B. W., B. D. Adair, C. Yoshioka, J. D. Quispe, G. Orca, P. Kuhn, R. A. Milligan, M. Yeager, and M. J. Buchmeier.** 2006. Supramolecular architecture of severe acute respiratory syndrome coronavirus revealed by electron cryomicroscopy. J. Virol. **80:**7918–7928.
39. **Ontiveros, E., L. Kuo, P. S. Masters, and S. Perlman.** 2001. Inactivation of expression of gene 4 of mouse hepatitis virus strain JHM does not affect virulence in the murine CNS. Virology **289:**230–238.
40. **Parker, M. M., and P. S. Masters.** 1990. Sequence comparison of the N genes of five strains of the coronavirus mouse hepatitis virus suggests a three domain structure for the nucleocapsid protein. Virology **179:**463–468.
41. **Peng, D., C. A. Koetzner, and P. S. Masters.** 1995. Analysis of second-site revertants of a murine coronavirus nucleocapsid protein deletion mutant and construction of nucleocapsid protein mutants by targeted RNA recombination. J. Virol. **69:**3449–3457.
42. **Peng, D., C. A. Koetzner, T. McMahon, Y. Zhu, and P. S. Masters.** 1995. Construction of murine coronavirus mutants containing interspecies chimeric nucleocapsid proteins. J. Virol. **69:**5475–5484.
43. **Peng, T. Y., K. R. Lee, and W. Y. Tarn.** 2008. Phosphorylation of the arginine/serine dipeptide-rich motif of the severe acute respiratory syndrome coronavirus nucleocapsid protein modulates its multimerization, translation inhibitory activity and cellular localization. FEBS J. **275:**4152–4163.
44. **Robbins, S. G., M. F. Frana, J. J. McGowan, J. F. Boyle, and K. V. Holmes.** 1986. RNA-binding proteins of coronavirus MHV: detection of monomeric and multimeric N protein with an RNA overlay-protein blot assay. Virology **150:**402–410.
45. **Robinson, C. R., and R. T. Sauer.** 1998. Optimizing the stability of single-chain proteins by linker length and composition mutagenesis. Proc. Natl. Acad. Sci. USA **95:**5929–5934.
46. **Rottier, P. J. M., G. W. Welling, S. Welling-Wester, H. G. M. Niesters, J. A. Lenstra, and B. A. M. Van der Zeijst.** 1986. Predicted membrane topology of the coronavirus protein E1. Biochemistry **25:**1335–1339.
47. **Saikatendu, K. S., J. S. Joseph, V. Subramanian, B. W. Neuman, M. J. Buchmeier, R. C. Stevens, and P. Kuhn.** 2007. Ribonucleocapsid formation of severe acute respiratory syndrome coronavirus through molecular action of the N-terminal domain of N protein. J. Virol. **81:**3913–3921.
48. **Sambrook, J., and D. W. Russell.** 2001. Molecular cloning: a laboratory manual, 3rd ed. Cold Spring Harbor Laboratory Press, Cold Spring Harbor, NY.
49. **Stohlman, S. A., R. S. Baric, G. N. Nelson, L. H. Soe, L. M. Welter, and R. J. Deans.** 1988. Specific interaction between coronavirus leader RNA and nucleocapsid protein. J. Virol. **62:**4288–4295.
50. **Sturman, L. S., K. V. Holmes, and J. Behnke.** 1980. Isolation of coronavirus envelope glycoproteins and interaction with the viral nucleocapsid. J. Virol. **33:**449–462.
51. **Takeda, M., C.-K. Chang, T. Ikeya, P. Guntert, Y.-H. Chang, Y.-L. Hsu, T.-H. Huang, and M. Kainosho.** 2008. Solution structure of the C-terminal dimerization domain of SARS coronavirus nucleocapsid protein solved by the SAIL-NMR method. J. Mol. Biol. **380:**608–622.
52. **Vennema, H., G.-J. Godeke, J. W. A. Rossen, W. F. Voorhout, M. C. Horzinek, D.-J. E. Opstelten, and P. J. M. Rottier.** 1996. Nucleocapsid-independent assembly of coronavirus-like particles by co-expression of viral envelope protein genes. EMBO J. **15:**2020–2028.
53. **Verma, S., V. Bednar, A. Blount, and B. G. Hogue.** 2006. Identification of functionally important negatively charged residues in the carboxy end of mouse hepatitis coronavirus A59 nucleocapsid protein. J. Virol. **80:**4344–4355.
54. **Verma, S., L. A. Lopez, V. Bednar, and B. G. Hogue.** 2007. Importance of the penultimate positive charge in mouse hepatitis coronavirus A59 membrane protein. J. Virol. **81:**5339–5348.
55. **White, T. C., Z. Yi, and B. G. Hogue.** 2007. Identification of mouse hepatitis coronavirus A59 nucleocapsid protein phosphorylation sites. Virus Res. **126:**139–148.
56. **Wilson, L., P. Gage, and G. Ewart.** 2006. Hexamethylene amiloride blocks E protein ion channels and inhibits coronavirus replication. Virology **353:**294–306.
57. **Wilson, L., C. McKinlay, P. Gage, and G. Ewart.** 2004. SARS coronavirus E protein forms cation-selective ion channels. Virology **330:**322–331.
58. **Ye, R., C. Montalto-Morrison, and P. S. Masters.** 2004. Genetic analysis of determinants for spike glycoprotein assembly into murine coronavirus virions: distinct roles for charge-rich and cysteine-rich regions of the endodomain. J. Virol. **78:**9904–9917.
59. **Yu, I.-M., C. L. T. Gustafson, J. Diao, J. W. Burgner II, Z. Li, J. Zhang, and J. Chen.** 2005. Recombinant severe acute respiratory syndrome (SARS) coronavirus nucleocapsid protein forms a dimer through its C-terminal domain. J. Biol. Chem. **280:**23280–23286.
60. **Yu, I.-M., M. L. Oldham, J. Zhang, and J. Chen.** 2006. Crystal structure of the severe acute respiratory syndrome (SARS) coronavirus nucleocapsid protein dimerization domain reveals evolutionary linkage between corona- and arteriviridae. J. Biol. Chem. **281:**17134–17139.
61. **Zhou, M., and E. W. Collisson.** 2000. The amino and carboxyl domains of the infectious bronchitis virus nucleocapsid protein interact with 3′ genomic RNA. Virus Res. **67:**31–39.